Precision Agriculture
https://doi.org/10.1007/s11119-018-9596-z

Mapping within-field variability in wheat yield and biomass using remote sensing vegetation indices

Isidro Campos[1,2] · Laura González-Gómez[1] · Julio Villodre[1] · Maria Calera[2] · Jaime Campoy[1] · Nuria Jiménez[3] · Carmen Plaza[2] · Sergio Sánchez-Prieto[1] · Alfonso Calera[1]

Abstract

This paper explored the ability of remote sensing (RS) and meteorological data to map the variability of yield/biomass in cultivated wheat (*Triticum aestivum*). The methodology integrated a time series of RS-based vegetation indices (VI) into a simple model based on the water productivity. Thus, the study analyzed if the biophysical parameters deduced from the VI could be used for the quantification of the differences in crop growth and yield assuming that in operative scenarios, the spatial distribution of the factors limiting the crop growth is unknown. The results of the model were analyzed in terms of the absolute values and the within-field variability with respect to space-continuous measurements of yield and biomass data. The variability registered in the fields was quantified as the ratio between actual yield or biomass in any given location and the mean value for the analyzed variable in each field. The good correlation between measured and modelled variability demonstrated the potential of the proposed approach to reproduce variability even under stress conditions. The proposed approach defined differences in crop growth similar to the ground measurements. The additional evidence obtained point to the necessity of considering the individual time-trajectory of each pixel for the assessment of within field variability. This approach requires the identification of the beginning and the end of the growing cycle. The proposed methodology, based on thresholds of VI offered promising results.

Keywords NDVI · Crop coefficient · Water use efficiency · AQUACROP

✉ Isidro Campos
campos.isidro@gmail.com

[1] GIS and Remote Sensing Group, Instituto de Desarrollo Regional, Universidad de Castilla-La Mancha, Campus Universitario SN, Albacete, Spain

[2] AGRISAT-IBERIA, Pol. Campollano, Av, 1ª N 18, Albacete, Spain

[3] ALIARA AGRÍCOLA, C/Matadero 11, Talavera de la Reina, Spain

Published online: 11 August 2018

Introduction

Precision farming emerged as an innovation driven solution (Dixon and McCann 1997) for the improvement of resource use efficiency in agriculture. Precision farming requires technology necessary for the distribution of the inputs and knowledge of the spatial distribution of crop requirements and their variability. Thus, site-specific maps of crop variability are necessary as an indicator of the response of the crops to certain factors (Arslan and Colvin 2002a). Maps of crop variability over a number of seasons provide site-specific information about the permanent factors (mainly climate and soil properties) and management factors (nutrients supply, pest problems or irrigation uniformity in irrigated lands) that affect the productivity. Thus, the application rates of the agronomic inputs (seeding rates, water and fertilizers) can be adapted to the actual demand, which is the paradigm of precision agriculture.

Possible alternatives for mapping the crop variability are the application of crop growth models (CGMs), electrical conductivity maps, the use of combine-mounted yield monitors and a family of diagnostic approaches based on remote sensing data (RS). The family of methods based on RS for the assessment of crop production includes the assimilation of RS-based biophysical parameters in the growth engine of the most common CGMs and direct-empirical relationships with the crop yield (Sadras et al. 2015). In the first group of methods, the biophysical parameters based on RS are incorporated as forcing variables into the CGMs. Some examples can be found in Zwart and Bastiaanssen (2007), Padilla et al. (2011) and Sibley et al. (2014). The second group is based on regressions between RS data obtained for a representative date and biomass or yield data. Examples of this methodology are the work done by Cicek et al. (2010) and Panda et al. (2010).

The regression approaches are mainly oriented to the determination of the average yield at the field or regional scales (Lobell and Azzari 2017; Lobell et al. 2015), but some authors have proposed the use of empirical relations with RS data for the assessment of within-field variability in crop yield and growth. Using this approach, Dang et al. (2011) proposed a regression model for the determination of the yield at pixel scale and the determination of potentially constrained sub-regions of fields that failed consistently to reach a specific yield quantile. Dalla Marta et al. (2013) found a positive relationship between spectral vegetation indices (VI) and yield related parameters for wheat during the stem elongation phases. These relationships indicated the capability of the VI to capture the variability of crop growth and production. Using a calibrated satellite regression model, Burke and Lobell (2017) explained between 15 and 40% of the variation in yields at field scale in Kenya. In a slightly different approach, Dobermann and Ping (2004) proposed the integration of VI acquired during the crop growth cycle and yield monitor data to improve the accuracy of combine-mounted yield monitors and the delimitation of yield patterns.

The barriers to the use of RS data for these tasks are essentially the same as already raised in other applications: resolution (spatial, temporal and radiometric), calibration, costs (Moran et al. 1997), the computational load issues when using large datasets and the capability to provide information in the appropriate format and time. However, the success of RS approaches for the assessment of the vegetation vigor has not been discussed (Dang et al. 2011) and according to available literature, the relationship between crop vigor at certain stages and final yield is positive in most cases. From a different point of view, the main weakness of these methods is the representativeness of one or a few images to reproduce a dynamic and accumulative process, as is the case of the yield/biomass production. It is fair to assume that the differences found in certain stages can be compensated (or at least

mitigated), reaching different vigor latterly, or varying the length of the growing season. In addition, the selection of the date (development stage) for the assessment of variability has an important impact on the capability to determine differences in canopy development. Aparicio et al. (2000) demonstrated the poor performance of various vegetation indices for explaining the differences in wheat yield if the images were obtained for a leaf area index greater than 3. These effects can be overcome if the methods consider the information contained in the temporal evolution of the RS data during the whole crop cycle, rather than single dates or short periods.

This work proposed the use of the temporal evolution of the RS data during the whole crop cycle for the assessment of crop growth variability at the scale of commercial farms, promoting the necessity of continuous monitoring of the crop biophysical parameters for a precise estimation of the spatial variability of crop growth. A preliminary version of this research was presented in the 11th European Conference of Precision Agriculture (Campos et al. 2017a). However, the present work expanded the number of fields analyzed, introduced the analysis of the spatial variability in yield and biomass production as the key variables and analyzed the aptitude of the model under severe water limited conditions, as is the case of rainfed wheat in the study area.

The methodology proposed integrates a time series of VI into the AQUACROP crop growth and yield partitioning model (Steduto et al. 2009) popularized by the FAO-66 manual (Steduto et al. 2012). This approach was applied to commercial fields planted with wheat and managed in irrigated and rainfed conditions. The performance of the proposed approach was evaluated in two ways. Initially, the variability estimated by the model was evaluated versus the variability based on the yield maps obtained by combine-mounted grain yield monitors. The second evaluation was the comparison of the variability estimated by the model versus the variability based on field measurements of aboveground biomass in areas with differences in crop growth. Considering that the crop variability can be affected by additional stresses not accounted for by the temporal evolution of VIs, the ability of the proposed approach to determine the spatial patterns in crop growth was analyzed in severe water limited conditions, as is the case of the rainfed fields in the study area (Southeast Spain).

Materials and methodology

Study sites

The data analyzed in this work were obtained in commercial fields located in the province of Albacete (Southeast Spain). The climate in the area is Mediterranean. The mean annual precipitation for the last 30 years is 340 mm and the mean annual temperature is 13.6 °C for the same period. The fields were managed under irrigation and rainfed conditions. All irrigated fields (fields 1–5) used center pivot systems and except for field 3, all monitored fields were managed under no-tillage and direct seeding. The growing season went from January to July for the irrigated varieties (spring wheat) and from November to June for the rainfed varieties (winter wheat). The irrigation timing varied from weekly events at the beginning of the season to daily applications during May. In spring irrigated wheats, fertilizer was applied in split portions at different stages during crop development, following local practices. In rainfed winter wheats, fertilizer was applied in two portions, before

seeding and during tillering. For additional information about the management, inputs and yield production see Table 1.

In addition to the natural variability of soil fertility, additional variability was induced in the crop growth by varying the N doses proposed by the farmer in selected locations for some fields via irrigation pivots during initial growth stages (crop emergence). During 2015 (fields 1, 3 and 4), the N doses were increased and reduced by 46 kg N ha^{-1} in two strips crossing the monitored fields. During 2016, the N dose in field 2 was reduced by 100 kg of urea (46 kg N ha^{-1}) in a strip crossing the field. The width of the strips (100 m) was sufficient to be monitored with the available images (Landsat 8 and Sentinel 2). As presented in the "Results", the crop response varied depending on the soil properties in the areas with homogeneous treatments and the proposed approach was able to detect the actual variability under homogeneous managements. The consequences of these treatments in the crop productivity and nitrogen use efficiency were not analyzed in this work.

Basis of the model for the estimation of the variability of yield and biomass production

Previous studies (Campos et al. 2017b, 2018) proposed that the assessment of biomass and yield production is the incorporation of the reflectance-based basal crop coefficient (Neale et al. 1989) into the AQUACROP crop growth and yield partitioning model (Steduto et al. 2009) popularized by the FAO-66 manual (Steduto et al. 2012). In this work, the same principles was applied, using the concept of normalized water productivity proposed in AQUACROP and the integration of reflectance-based crop coefficients, for the assessment of the within-field variability in crop growth. For simplicity, this methodology was named spatial variability based on vegetation indices. According to the FAO-66 methodology, biomass is estimated as the product of a normalized water productivity (WP^*, in g m^{-2}) (Steduto et al. 2007) times the summation of the ratio between actual crop transpiration (T_{ca}) over the reference evapotranspiration (ETo), (see Eq. 1). The ratio of T_{ca} over ETo is equivalent to the actual transpiration coefficient (K_{ta}).

$$Biomass = WP^* \cdot \sum_{to}^{t} \frac{T_{ca}}{ETo} = WP^* \cdot \sum_{to}^{t} K_{ta} \tag{1}$$

The formulation presented in the Eq. 1 only considers the effect of water stress reducing the crop transpiration (actual transpiration) and the biomass productivity. However, the biomass production is dynamic and can change during the growing cycle because of factors related to the meteorological conditions and the crop physiology and management. These factors can be represented by a variety of stress coefficients. Explicitly, the FAO-66 methodology considers the temperature and fertility stress coefficients, K_{st} and K_{sf} respectively (see Eq. 2). The term K_{ta} can be estimated as the product of the water stress coefficient (K_{sw}) times the crop transpiration coefficient (K_t). The coefficient K_t is the ratio of crop transpiration to atmospheric demand under non-limiting moisture conditions. This is similar to the basal crop coefficient (K_{cb}) defined by Allen et al. (1998) but different because K_{cb} includes residual soil evaporation and thus exceeds K_t under partial cover conditions. For additional discussion about the convenience of minimum K_t values equal or greater than 0 for the assessment of biomass production, the reader is referred to Campos et al. (2017c). The FAO-66 methodology estimates crop yield as a variable proportional of the crop biomass (see Eq. 3). The ratio between yield and biomass is the harvest index (HI). In

Table 1 Summary of the management and ground data acquired in fields analyzed in this work

Field ID	Year	Location	Management	Variety	Irrigation (mm)	Fertilization, kg (N; P; K)	Yield (t ha^{-1})	Harvest Index	Biomass data
1	2015	39.2521; – 1.9983	Irrigated, direct seeding	Califa sur	452	(257; 81; 65)	8.82	0.52	9 plots
2	2016	39.2528; – 1.9903	Irrigated, direct seeding	Califa sur	453	(218; 105; 34)	7.51	0.43	8 plots
3	2015	38.8743; – 1.8373	Irrigated, conventional	Califa sur	447	(268; 120; 150)	7.45	0.49	9 plots
4	2015	39.0795; – 1.6574	Irrigated, direct seeding	Galera	230	(140; 79; 0)	4.03	0.41	9 plots
5	2016	39.0632; – 16752	Irrigated, direct seeding	Galera	240	(11; 0; 0)	5.03	0.38	6 plots
6	2016	39.2793; – 1.9750	Rainfed, direct seeding	Pr22–Pr23	–	(80; 51; 0)	3.12	0.35	No data
7	2016	39.2808; – 1.9778	Rainfed, direct seeding	Sarina	–	(80; 51; 0)	3.44	0.35	No data
8	2016	39.2693; – 1.9662	Rainfed, direct seeding	Sarina	–	(80; 51; 0)	3.00	0.38	3 plots

absence of stresses or limitations, every stress coefficient is equal to 1 and the biomass production is proportional to the sum of K_t during the growing cycle. By the same definition, the sum of the products $WP^* \cdot K_t$ and $WP^* \cdot K_t \cdot HI$ provides an estimation of the potential biomass and yield production, respectively.

$$Biomass = WP^* \cdot \sum_{to}^{t} K_{ta} \cdot K_{st} \cdot K_{sf} = WP^* \cdot \sum_{to}^{t} K_t \cdot K_{sw} \cdot K_{st} \cdot K_{sf} \quad (2)$$

$$Yield = HI \cdot Biomass \quad (3)$$

The feasibility of using the RS-based K_t for the assessment of biomass production in wheat, corn and soybean has been demonstrated in previous experiments (Campos et al. 2017b, 2018). However, under stress conditions, the spatial scale of the input parameters (mainly soil properties) must be fine enough for the assessment of the variability in the stresses affecting the crop growth at the sub-field scale. This work analyzed if RS-based K_t could be used for the quantification of the differences in crop growth and if these differences can be translated into the variability in potential yield/biomass production. The hypothesis behind this assumption is that, for the same crop during the same growing season in a small area, as is the case of an agricultural plot, the differences in canopy development can be attributed to the lack of management uniformity, pests or diseases and the soil fertility, expressed in terms of mineral nutrition and water availability. If the application of fertilizers and water (for irrigated crops) is homogeneous at the plot scale, the differences in the actual growth are exclusively attributable to the soil fertility and the presence of pests or diseases. This paper proposes a simplified approach for which the stresses affecting the yield/biomass production are considered unknown and the within-field variability is estimated exclusively based on the accumulated value of RS-based K_t. The only stress considered is the cold stress coefficient because it can be estimated in operative applications just using air temperature data. Although this stress can be considered homogeneous at the scale of a commercial farm, its effect on the biomass accumulation could be different depending on the actual development of each area monitored during the stress periods. The actual yield or biomass production may be lower than this potential but the main objective of this work is the analysis of the spatial heterogeneity at the sub-field scale quantified as variability in yield and biomass production. The procedure followed is summarized in Fig. 1.

Parameterization of the spatial variability model based on vegetation indices

Water productivity, transpiration coefficient and temperature stress coefficient

One of the main weaknesses of almost every CGM for the assessment of the in-field variability in yield and biomass is the determination of crop transpiration, light interception or, specifically, K_t in the AQUACROP approach. A time series of RS data offers a unique way to monitor the spatial distribution of K_t during the whole growing season. For this purpose, the relationship between the VI and the K_t has been proposed. This study was based on the relationship proposed by Duchemin et al. (2006) for wheat using the normalized difference vegetation index (NDVI), see Eq. 4.

$$K_T = 1.64 \cdot (NDVI - 0.14) \quad (4)$$

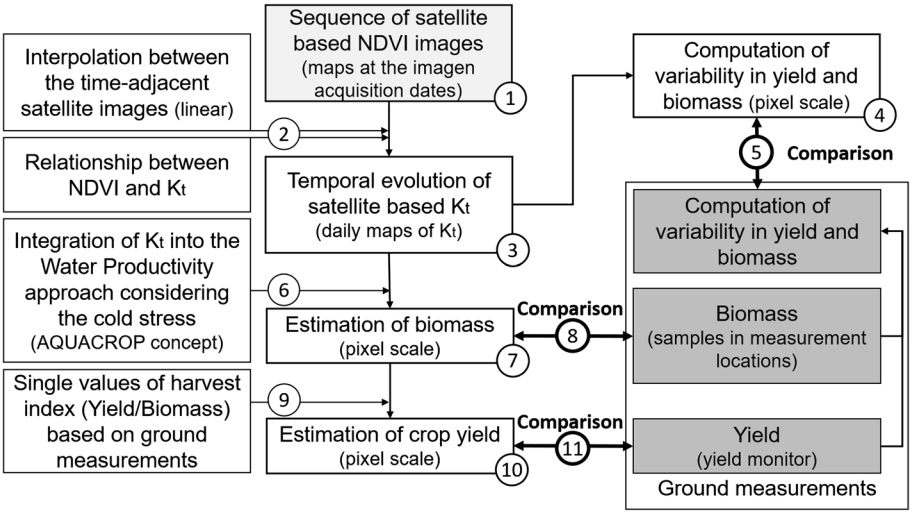

Fig. 1 Flow diagram of the procedures followed for the estimation and evaluation of yield and biomass in wheat and the within-field variability of both variables. The numerical labels show the order of operations

As indicated earlier, the only stress considered in this work is K_{st} and it was calculated following Eq. 5 (Raes et al. 2011). The formulation of K_{st} is based on the growing degree days (GDD), calculated as the difference between average daily temperature and the base temperature for the crop monitored, 0 °C for wheat. The estimation of K_{st} requires knowledge of the upper and lower thresholds of GDD to produce biomass, these thresholds are 0 and 13 °C for wheat (Raes et al. 2011).

$$K_{st} = \frac{\left(S_n \cdot S_x\right)}{S_n + \left(S_x - S_n\right) \cdot \exp^{-r(1-Srel)}} \tag{5}$$

where S_x and S_n are the upper and the lower limits of K_{st} and were assumed equal to 1.0 and 0.01 respectively; S_{rel} is the relative stress level, S_{rel} is 0.0 and 1.0 at the upper and lower threshold of GDD, 13 and 0 °C respectively; r is the rate factor (16.5).

The values of $\Sigma K_t \cdot K_{st}$ at the pixel scale were converted into biomass production by multiplying by a fixed value of WP*. The WP* used in this work (17.9 g m^{-2}) was based on the model calibration proposed by Campos et al. (2018) for wheat in the province of Albacete (Southeast Spain) and it is within the range proposed by Raes et al. (2011) for wheat.

The yield (grain) production was estimated as the product of the simulated biomass multiplied by HI measured in the field. The model results were analyzed with respect to the measurements of yield and aboveground biomass in g m^{-2}. As indicated before, the simulated values of ground biomass and yield calculated following the methodology described do not account for limiting conditions (water or nutrition stresses). Thus, the accuracy of these estimates was analyzed with respect to field measurements of above ground crop biomass and grain production based on the yield maps obtained by combine-mounted grain yield monitors (see the section on "Ground data and satellite images").

Definition of the growing cycle based on spectral vegetation indices

Biomass estimation is based on a sum for which the limits t_0 and t, the actual value of WP^* and the actual values of K_t must be known (see Eq. 2). The selection of t_0 and t was based on thresholds for the VI analyzed and calculated individually for each pixel. Using thresholds of the analyzed VI helps to delimit the length of the growing cycle and the time trajectory individually for each pixel (see Fig. 2). This methodology is different from the selection of t_0 and t based on calendar days, or alternative scales such as the thermal time for the whole field and could help to represent the expected variability in the crop development (grain maturity stage) and the final biomass accumulation. The ability of each approach (VI thresholds or fixed dates) to reproduce the actual variability measured in the field was analyzed for a selected data subset (field 2) in the sensitivity analysis presented in this work.

The selection of the NDVI threshold for the beginning of the biomass accumulation (t_0) was 0.3 and it is based on the detection of the green-up phase proposed by Lobell et al. (2013). The green-up occurs during the initial development phases (tillering stages). Although this phase does not coincide exactly with the beginning of the biomass accumulation (emergence), there was 2% uncertainty in the estimation of biomass accumulation.

The value of NDVI that defined the final biomass accumulation (t) was initially proposed as 0.4 although this value was analyzed in the sensitivity analysis. The final biomass accumulation coincides with the grain maturity for wheat crops. According to previous experience of directly observing wheat phenology, the physiological maturity of the grain occurs for NDVI values around 0.4 for irrigated wheat (González-Gómez et al. 2018). In the sensitivity analysis, the accuracy of the model was analyzed by varying the NDVI threshold that determines the end of the growing cycle (from 0.35 to 0.45) and by selecting the end of the growing cycle based on calendar dates (from 0 to 2 weeks before the harvest date).

The application of this methodology pixel by pixel and at the scale of a satellite image in an operational and simple way was solved using the software TONIpbp (Tool for Numerical Integration pixel by pixel), developed by the GIS and Remote Sensing Group from the University of Castilla-La Mancha in the frame of the project FATIMA (http://fatima-h2020.eu, last accessed October 2017).

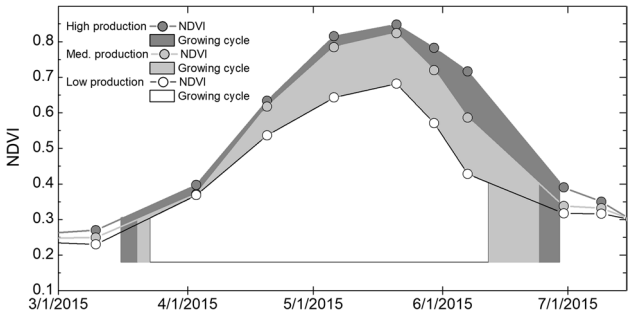

Fig. 2 Representation of how the growing cycle was delimited based on NDVI thresholds for 3 pixels with different production (high, medium and low) in field 3 (see "Ground data and satellite images" section)

Ground data and satellite images

The samples of aboveground biomass were collected at different measurement locations and dates during the growing season, see Table 1. Each sample was composed of 3 sub-samples. In each sub-sample, the aboveground biomass was manually collected for 1.5 m along 2 adjacent rows and dried in an oven for more than 48 h at 60 °C. Each of the measurement locations was situated in a homogeneous area with a minimum area of 1 ha. The homogeneous areas were delimited based on maps of potential biomass production obtained for previous crops following the model for spatial variability based on VI (described in "Parameterization of the spatial variability model based on vegetation indices").

The spatial distribution of the harvestable yield was mapped using a combine-mounted grain yield monitor (Trimble CFX750). The measurements of the yield monitor were calibrated against the total production weighed every 3–4 ha and spikes in yield detected at the beginning and the end of segments were removed manually. For quantitative analysis of the yield maps, the yield data points within an approximately 9 m^2 area were averaged. This is an area equivalent to 3 by 3 pixels of the maps based on RS data. This is a common strategy working with RS data due to the uncertainty in the geolocation of the pixels. The size of the pixels varied for the maps based on RS data in 2015 (30 m) and 2016 (10 m). The difference in the pixel size depended on the satellite images used in the model (Landsat 8 or Sentinel 2A).

The temporal evolution of the NDVI for every pixel in each field monitored was obtained from a time series of images acquired by the Landsat 8 and Sentinel 2A satellites. The images used in the analysis for each field are presented in Table 2. The maps of variability obtained during 2015 were based on Landsat 8 and the estimates of yield, biomass and variability were obtained at the scale of this sensor (30 m). The maps obtained during 2016 were mainly based on Sentinel 2A and the estimates of yield, biomass and variability were obtained at the scale of this sensor (10 m), although some images from Landsat 8 were also used during 2016 to increase the temporal resolution of the time series. As shown by Campos et al. (2018), the number of images must be enough to describe inflexion points of the growing cycle, thus the temporal distribution of the images through the growing cycle is more important than the number of images. For the integration of the different spatial resolutions during 2016, the software TONI resizes the Landsat pixel at the scale of Sentinel data and averages the NDVI values based on the original 30 m Landsat pixels. The effect of the atmosphere and the possible differences in the inter-calibration of the sensors were compensated for using a normalization procedure of the NDVI (Chen et al. 2005) based on pseudo-invariant surfaces (dense vegetation like alfalfa and agricultural bare soils).

The results of the model were analyzed in terms of yield, biomass and the within-field variability compared to the variability determined using ground measurements. The variability measured in the field was quantified as the ratio between actual yield or biomass in any given location and the mean value for the analyzed variable in the field. Equation 6 represents the estimation of the variability for the pixel i based on the yield measured in the pixel (Y_i) and the mean yield in the field monitored (Y_{avr}). This concept is equivalent to the normalized yield proposed by Stafford et al. (1996) for the comparison of the variability in grain production in a multi-annual analysis.

$$\text{Variability}_i = \frac{Y_i}{Y_{avr}} \tag{6}$$

Table 2 Dates (day/month) of the images used in the analysis

Field (year)	September–December	January–February	March	April	May	June	July
1 (2015)		14/01 (L8)	10/03 (L8)	20/04 (L8)	06/05 (L8)	07/06 (L8)	09/07 (L8)
					22/05 (L8)	30/06 (L8)	
2 (2016)		4/02 (S2)	05/03 (L8)	10/04 (S2)	01/05 (S2)	09/06 (L8)	03/07 (S2)
		21/02 (S2)	25/03 (S2)	14/04 (S2)	11/05 (S2)	20/06 (S2)	
				24/04 (S2)	31/05 (L8)	23/06 (S2)	
						25/06 (L8)	
						30/06 (S2)	
3 (2015)		14/01 (L8)	10/03 (L8)	20/04 (L8)	06/05 (L8)	07/06 (L8)	
					22/05 (L8)	30/06 (L8)	
4 (2015)		14/01 (L8)	10/03 (L8)	20/04 (L8)	06/05 (L8)	07/06 (L8)	09/07 (L8)
					22/05 (L8)	30/06 (L8)	
5 (2016)		17/01 (L8)			01/05 (S2)	10/06 (S2)	
		24/01 (L8)	12/03 (S2)	01/04 (S2)		13/06 (S2)	
		02/02(L8)	25/03 (S2)	14/04 (S2)	21/05 (S2)	16/06 (S2)	02/07 (L8)
		04/02 (S2)		24/04 (S2)	24/05 (S2)	20/06 (S2)	
						23/06 (S2)	
6, 7 and 8 (2016)	27/09 (L8)						
	13/11 (S2)	24/01 (L8)	12/03 (S2)	24/04 (S2)	01/05 (S2)	10/06 (S2)	
	03/12 (S2)	04/02 (S2)	25/03 (S2)		21/05 (S2)		
	16/12 (L8)						

L8 landsat 8, *S2* Sentinel 2 A

On the basis that WP* can be considered constant for the same crop under constant CO_2 concentrations (Steduto et al. 2007), the estimation of the variability in biomass production did not require a priori knowledge of WP* . The estimation of the variability in yield production requires the knowledge of the HI for each point analyzed. However, the spatial distribution of this factor should be considered unknown in operational applications and this value was considered constant for the whole field in this work. Consequently, the estimation of the variability in yield dod not require a priori knowledge of HI or WP* and it was exclusively based on the sum of the product $K_t \cdot K_{st}$. For the comparison of the results of the model and the ground measurements of biomass, the values calculated by the model were averaged over 1 ha around each measurement location. For the comparison with the yield maps, the values calculated by the model and based on the yield maps were averaged for an area equivalent to 3 by 3 pixels of the satellite images used in the model. In both cases, the field data were compared with the yield and biomass estimated by the model at grain maturity.

Results

Analysis of the proposed approach for the assessment of yield variability based on vegetation indices

The summary of the results in terms of measured and modeled values of yield and the statistics comparing the results in terms of yield and variability are presented in Table 3. Figure 3 shows the correlation between measured and modelled values of yield and variability and the corresponding r^2 and p values obtained for the linear regression. It should be noted that the r^2 and p values are the same for the correlations of biomass and variability data, hence a unique pair of values was represented in each graph.

The analysis of the linear regression indicated that the correlation between measured and modelled yield was significant for every field monitored ($p < 0.05$), although the values

Table 3 Summary of the results in terms of measured and modeled yield and statistics comparing the measured and modeled values of yield and variability for the areas monitored, excluding borders and unproductive zones like paths

Field ID	Yield monitor		Modeled values		RMSE		d	
	Yield average (t ha^{-1})	SD (t ha^{-1})	Yield average (t ha^{-1})	SD (t ha^{-1})	Yield (t ha^{-1})	Variability	Yield	Variability
1	8.82	0.47	8.91	0.20	0.37	0.04	0.63	0.64
2	7.51	0.43	7.52	0.29	0.34	0.04	0.64	0.64
3	7.45	0.52	7.29	0.23	0.42	0.05	0.61	0.61
4	4.03	0.76	3.99	0.60	0.27	0.07	0.83	0.83
5	5.03	0.37	4.75	0.40	0.42	0.06	0.42	0.57
6	3.12	0.36	4.74	0.32	1.65	0.09	−0.64	0.62
7	3.44	0.59	4.67	0.57	1.33	0.13	−0.20	0.62
8	3.00	0.28	4.49	0.34	1.53	0.09	−0.71	0.50

SD standard deviation, *RMSE* root mean square error, *d* improved index of agreement (Willmott et al. 2012) (fields 1–5 are irrigated and 6–8 are not)

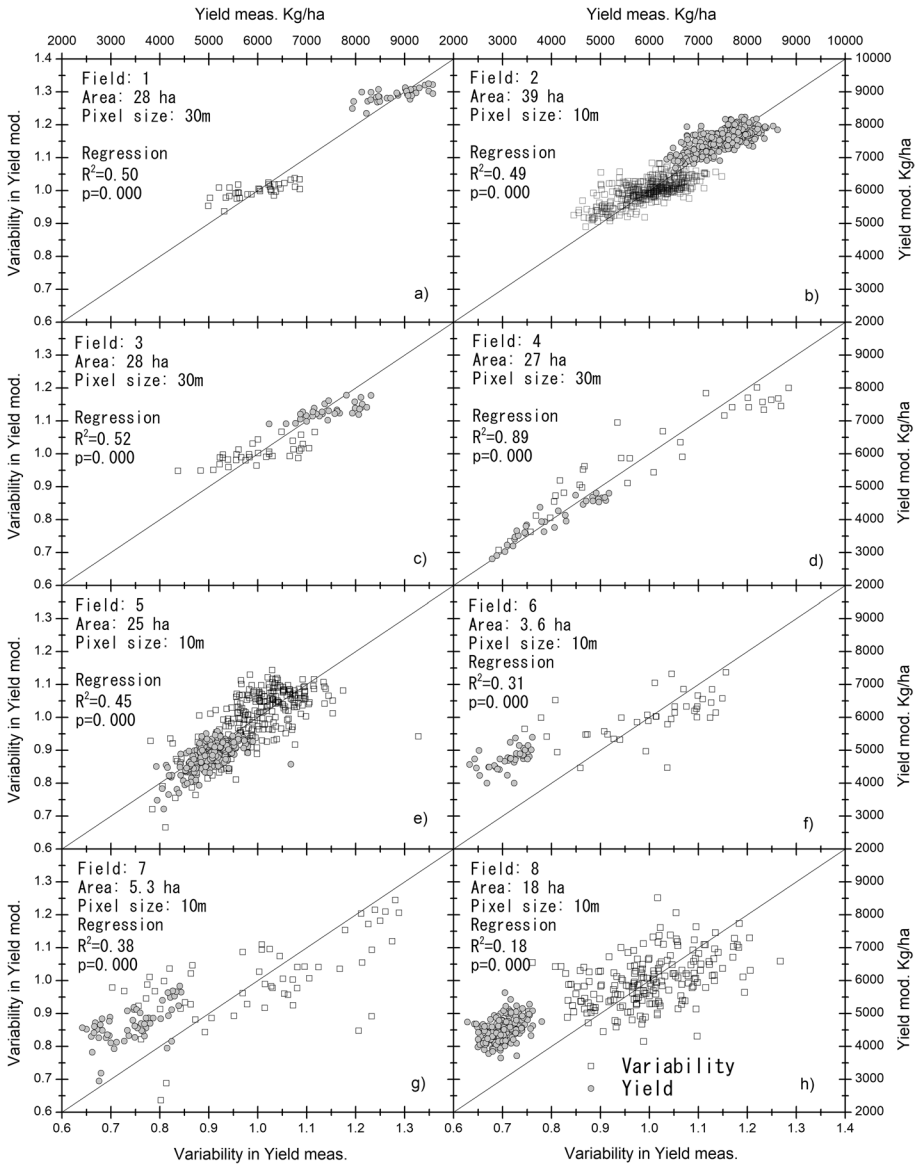

Fig. 3 Comparison of measured and modeled variability (left and bottom axes) and yield (right and top axes) based on field measurements (yield meas.) and the approach presented in Eqs. 2 and 3 (yield mod.). The graphs contain the r^2 and p value for the linear regressions between measured and modelled variables

of r^2 revealed a poor correlation for some fields as analyzed below (see Fig. 3). The correlation of the measured and modelled yield confirmed the potential of the model to reproduce the spatial patterns and the absolute yield values for the irrigated fields (fields 1–5). Conversely, the results indicated a clear overestimation of the yield for the unirrigated fields (see Fig. 3f–h). On the other hand, the values of the standard deviation (SD) presented in Table 3 indicate that the range of yield estimated by the model was, in general,

slightly lower that the measurements based on the yield monitor. This effect was evident for fields 1, 2 and 3 and is apparent in the correlations shown in Fig. 3a–c. For these fields, the model tended to overestimate the crop yield in the less productive areas and underestimate the actual yield in the more productive areas. These estimation biases had consequences in the comparison in terms of the variability.

The range of the variability based on the measured and modelled data was approximately 60% of the mean values for the most heterogeneous fields (fields 4, 6, 7 and 8). The variability estimated for the most homogeneous fields (fields 1, 2, 3 and 5) was less than 40% of the mean values (see Fig. 3). The correlation between measured and modelled variability (see Fig. 3) demonstrated the ability of the model for spatial variability based on VI to quantify the within-field variability at the spatial scales analyzed (i.e. 1 ha or finer resolution). The correlation between measured and modelled variability was significant also for the fields under deficit conditions, independently of the bias introduced by the assumption of the potential conditions in every field. However, it is fair to say that these results indicated that the proposed approach did not reproduce some of the effects affecting the spatial distribution of the crop yield, as indicated by the poor correlation coefficients obtained in the regressions, also in the case of irrigated fields (see Fig. 3). The accuracy of the model, quantified as the root mean square error (RMSE), indicates that the model was not able to reproduce about 13% of the measured variability in the fields cultivated under rainfed conditions (fields 6–8). The accuracy of the model was higher in the irrigated fields (fields 1–5), with the RMSE being lower than 7% of variability for each irrigated field.

The visual comparison of the yield maps and the maps derived from the proposed methodology (see Fig. 4) revealed the capability of the model for spatial variability based on VI to differentiate areas with differences in crop growth and production. As presented in the representation of field 4, the model was able to identify the area with higher production in a strip crossing the field from the Northwest to the Southeast. This strip coincides with the bottom of a valley between gentle slopes, thus the possible explanation of the higher productivity is greater soil fertility and water availability in this area. In field 7, the model denoted a linear pattern predicting higher production in the West of the field in agreement with the yield data obtained.

The sources of uncertainty in the model are the estimation of the spatial distribution of crop biomass and the possible uncertainty associated with the use of a fixed value of HI for the whole field. The ability of the proposed approach to reproduce the variability in biomass production is analyzed in the next subsection and the effect of a fixed value of HI is discussed in the "Discussion".

Analysis of the proposed approach for the assessment of biomass variability

The summary of the results in terms of measured and modeled values of biomass and the statistics comparing the results of biomass and biomass variability are presented in Table 4. Figure 5 represents the correlation between measured and modelled values of biomass and variability. The results corroborated the conclusions obtained for the analysis in terms of yield. The model provided a precise estimation of the biomass production for fields 1–5 (Fig. 5a–e), while the model overestimated the biomass production in field 8 under rainfed conditions (Fig. 5f). Biomass data was not available for fields 6 and 7. The RMSE comparing measured and modelled biomass was lower than 2.7 t ha^{-1} for every analyzed field and lower than 1.5 t ha^{-1} (around 10% of the average value) for the fields with higher productivity (irrigated fields).

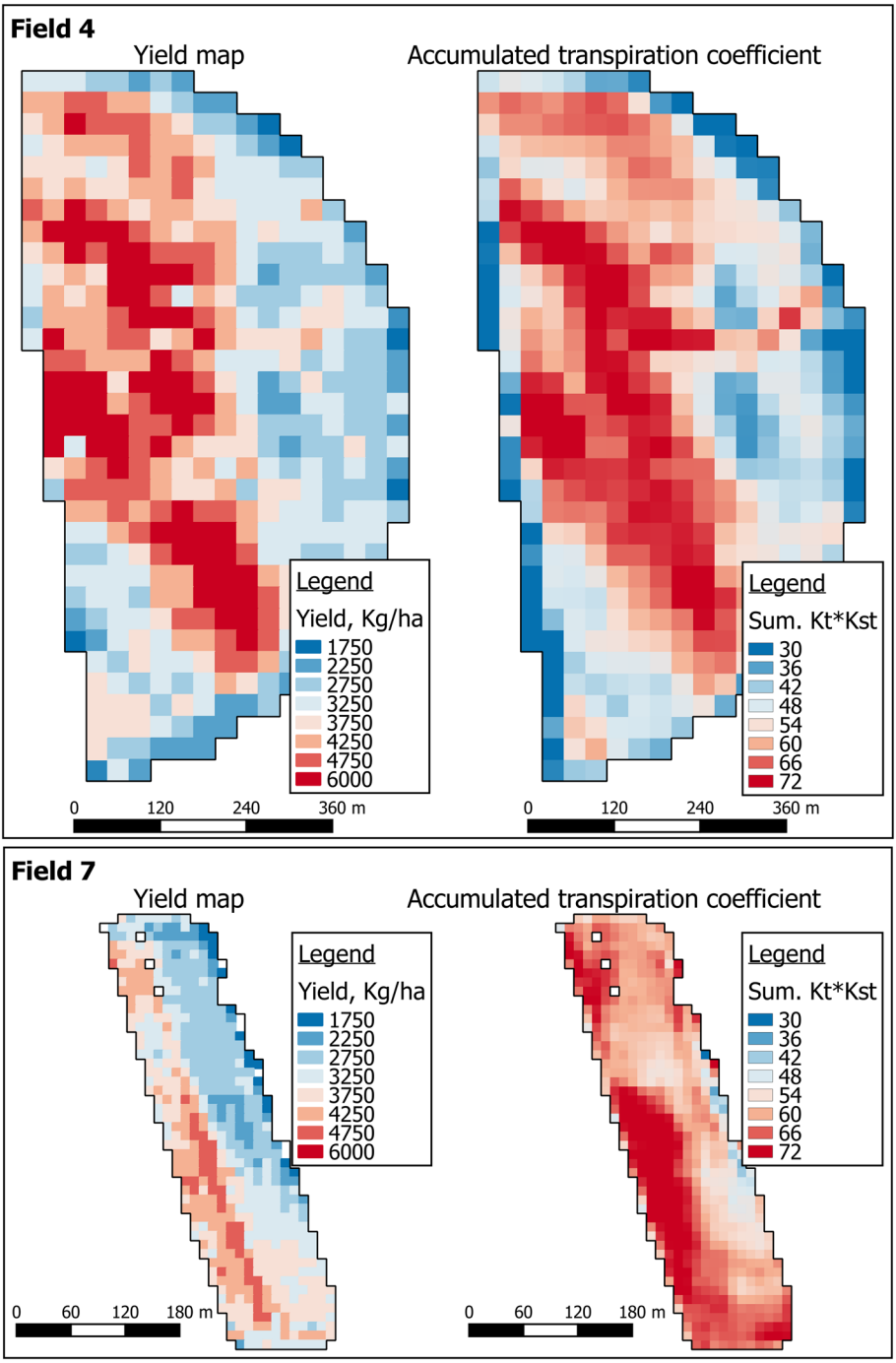

Fig. 4 Yield maps derived from the yield monitor and the accumulated value of the transpiration coefficient (K_t) times the temperature stress coefficient (K_{st}) for two selected fields (field 4 and field 7)

Table 4 Summary of the results in terms of measured and modeled biomass (Bio.) and statistics comparing the measured and modeled values of Bio. and variability (Var.)

Field ID	Ground measurements		Modeled values		RMSE		d	
	Mean biomass (t ha^{-1})	SD (t ha^{-1})	Mean biomass (t ha^{-1})	SD (t ha^{-1})	Biomass (t ha^{-1})	Variability	Biomass	Variability
1	17.52	1.90	17.55	0.43	1.49	0.09	0.60	0.60
2	16.21	1.37	17.34	1.01	1.39	0.05	0.44	0.63
3	14.21	1.52	14.76	0.71	1.45	0.09	0.48	0.54
4	10.98	2.89	11.30	2.05	1.46	0.13	0.73	0.75
5	13.95	0.76	14.30	0.69	0.44	0.03	0.69	0.71
8	8.39	0.28	11.01	0.96	2.69	0.06	−0.84	−0.03

SD standard deviation, *RMSE* root mean square error, *d* improved index of agreement (Willmott et al. 2012)

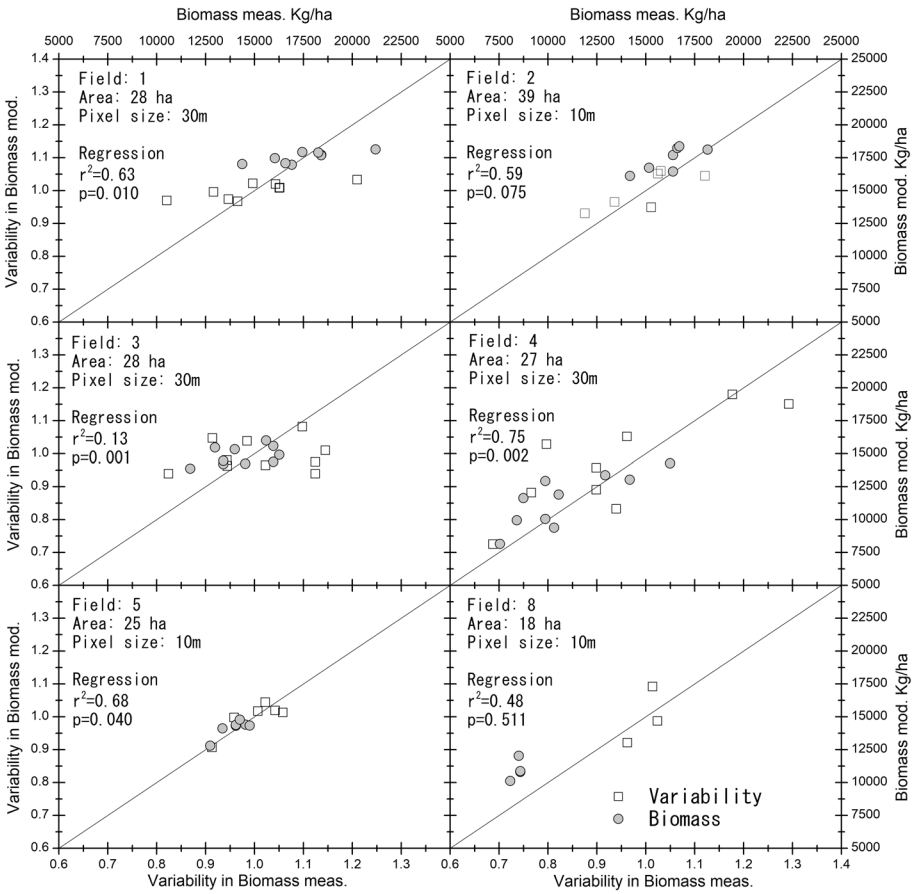

Fig. 5 Comparison of measured and modeled variability based on biomass (left and bottom axes) and biomass data (right and top axes) measured in the field (Biomass meas.) and modelled following Eq. 2 (Biomass mod.). The graphs contain the r^2 and p values for the linear regressions between measured and modelled variables

The comparison indicated that, in general terms, the SD was greater for the biomass based on ground data, these results were evident for fields 1, 2 and 3. The variability based on biomass data was less than 60% of the mean values for the most heterogeneous fields (fields 1 and 4) and less than 40% of the mean values for the most homogeneous fields (fields 2, 3, 5 and 8) (see Fig. 5). The accuracy of the model as quantified by the RMSE indicated that the model was not able to reproduce about 13% of the measured variability in the most heterogeneous field (RMSE = 0.13 in field 4). In the most homogeneous fields (fields 2, 3, 5 and 8), the RMSE was lower than 0.09. The correlation between measured and modelled variability (Fig. 5) pointed to the good performance of the proposed approach at reproducing the within-field variability in terms of biomass. The analysis of the r^2 and p values obtained for the regressions point to the necessity of improving estimations of biomass and variability only in fields 2 and 8, although the values of these statistics could be biased by the low range of the variables correlated (Willmot 1982).

In view of the results, the model reproduced most of the variability registered in every measurement location in fields 2, 3, 4, 5 and 8 with reasonable accuracy. The variability calculated for the biomass data differed from the modelled values only in some extreme points for field 1 (see Fig. 5). It should be noted that field 1 was not within the most heterogeneous fields in terms of yield (see Fig. 3), but some extreme values obtained in the biomass measurements increased the actual range of variability based on biomass data. The possible explanation for these differences is that the spatial representativeness of the biomass measurements could introduce additional uncertainty which is addressed in the discussion section.

Selection of the NDVI threshold for the definition the growing cycle

The results of the sensitivity analysis indicated that the selection of various alternatives for the definition of the end of the growing cycle, represented by the variable t in Eq. 2, affected the accuracy of the model in reproducing the crop yield. In general terms, the applications of the model based on fixed dates (0, 1 or 2 weeks before harvest) resulted in the poorest performance in terms of yield in comparison to the applications based on thresholds of the NDVI (0.35, 0.4 or 0.45) for each pixel, see Table 5. In contrast, the sensitivity analysis was not clear in determining the most accurate approach (NDVI thresholds

Table 5 Statistics comparing the results of the model in terms of measured and modeled yield and variability for different approaches to the selection of the end of the growing cycle in field 2

	Yield data (t ha^{-1})			Variability	
	RMSE	MBE	d	RMSE	d
Weeks before harvest					
−2	0.34	−0.13	0.62	0.042	0.65
−1	0.42	−0.27	0.53	0.042	0.65
0	0.50	−0.38	0.42	0.042	0.64
NDVI threshold					
0.35	0.33	−0.01	0.64	0.044	0.64
0.40	0.34	−0.07	0.64	0.044	0.64
0.45	0.34	−0.13	0.62	0.042	0.64

RMSE root mean square error, *MBE* mean bias error, *d* improved index of agreement (Willmott et al. 2012)

versus fixed dates) for the assessment of the spatial variability. The statistics comparing measured and modelled variability were similar in terms of RMSE and d for the different approaches proposed for the selection of t.

Given the results of the sensitivity analysis, the methodology based on the threshold of NDVI equal to 0.4 was selected in this work. In the field analyzed in this section (field 2), the threshold equal to 0.45 produced more precise estimates, however this threshold seems to be excessive for the rainfed fields monitored in this work. The approach based on thresholds was shown to be more precise than fixed dates in reproducing yield values and the threshold equal to 0.4 agrees with NDVI values observed at physiological maturity of wheat grain in the study area (González-Gómez et al. 2018). The identification of physiological maturity using the NDVI threshold proposed by González-Gómez et al. (2018) is based on few experiments (20 commercial fields monitored during 10 growing seasons) and could vary for different varieties and management approaches.

Discussion

Strengths and weakness of the model for spatial variability based on vegetation indices

The results obtained in this work revealed the potential of the proposed approach for assessing within-field variability in cultivated wheat. The analysis of the results indicated that an accurate estimation of crop biomass and yield production requires consideration of the stresses affecting these processes. The RMSE comparing measured and modelled yield was lower than 0.45 t ha^{-1} in the irrigated fields (fields 1–5) while the RMSE increased up to about 1.3 t ha^{-1} in the rainfed fields (fields 6–8) due to the presence of water stress. The RMSE comparing measured and modelled biomass data was lower than 1.5 t ha^{-1} in irrigated fields (fields 1–5) while the RMSE increased up to around 2.7 t ha^{-1} in the rainfed field (field 8). The RMSEs comparing measured and modelled yield and biomass in irrigated fields were within the range obtained by more complex approaches. Similarly, Iqbal et al. (2014) obtained a RMSE of 0.9 t ha^{-1} for biomass and 0.58 t ha^{-1} for yield with the AQUACROP model calibrated in experimental plots (5 m × 10 m). Jin et al. (2017) obtained a RMSE over 1.53 t ha^{-1} when simulating biomass and 0.81 t ha^{-1} for simulated yield. Their studies were at the regional scale (40 samples) using the AQUACROP model calibrated for the study area. In addition, the model assimilates remote sensing estimates of ground cover (optical and radar) in an iterative approach that modifies the model parameterization for the best fitting remote sensing estimates. Using the same model calibrated for the study area, Jin et al. (2014) obtained RMSEs of 1.29 t ha^{-1} and 0.52 t ha^{-1} simulating biomass and yield, respectively. According to the literature review, the proposed approach did not significantly improve the accuracy of previous approaches; however, the analyses of the variability demonstrated the potential of the model to account for the heterogeneity measured in the field. The values of d and RMSE pointed to a clear improvement in model accuracy when the data were analyzed in terms of variability compared to analyses in terms of yield (see Table 3). In general, the analysis of variability increased the values of d and reduced the ratio between the RMSE and the mean values. This effect was more evident in the rainfed fields.

As indicated in the results section, the main sources of uncertainty for the simulation of the within-field variability are the possible effect of the stresses not considered in the

proposed approach and the consideration of a fixed value of the harvest index. The most common stresses in the study area are water and nitrogen deficits. Both stresses affect the processes of yield and biomass accumulation in two ways: controlling plant growth (expansion) and reducing the efficiency of the biomass production process. The reduction in plant growth-expansion occurs in the initial phases of the stresses. These effects have been quantified for wheat in terms of leaf development and tillering (Longnecker et al. 1993; Maas and Grieve 1990) or light interception at canopy scale (Garcia et al. 1988). While the stress conditions develop and the deficit is more evident, the plants react reducing the efficiency of the biomass production process and it is generally accepted that the reduction of plant expansion occurs prior to the limitations on biomass efficiency (Ings et al. 2013; Jamieson et al. 1998; Ritchie et al. 1998).

The use of the accumulated value of the reflectance based K_t as an indicator of the various stresses affecting plant expansion is qualitatively equivalent to the experimental measurement of these effects. However, the stresses that reduce the efficiency of yield and biomass production could affect the accumulation of biomass beyond canopy expansion, adding uncertainty to the estimates based on the proposed approach. From the results obtained in this work, the accumulated value of K_t reflected most of the variability measured in the fields, including fields under severe water stress conditions. The assumption that the zones with lower plant expansion are exposed to higher stress levels for biomass production seems to be a reasonable hypothesis. It is fair to say that in the analyzed fields, stresses occurred during most of the growing cycle, reducing the canopy expansion and the duration of the cycle. However, the performance of the proposed approach should be analyzed under different conditions. In particular, the performance of the proposed approach must be analyzed when the stresses occur at the end of the growing cycle, when most of the crop structure has been developed and the stresses exclusively affect the accumulation of yield. The approach selected in this study was exclusively based on the K_t derived from RS images and the maximum and minimum daily air temperatures used for the estimation of K_{st}. Thus, the methodology can be easily evaluated in other agronomic areas using RS images and ground meteorological stations. Alternatively, the application of this approach in areas with low availability of ground data can be based on air temperature estimates based on satellite platforms, but the uncertainties associated with the data sources should be analyzed. Other interesting variations in the proposed approach are the use of biomass production models based on light use efficiency and water productivity. It should be noted that the selection of the most adequate approach for the simulation of the biomass production in each crop and area is still an open discussion. However, different approaches have been demonstrated to be equivalent to the one reported here for the simulation of the wheat biomass production in Albacete (Spain) (Campos et al. 2018) and similar performance in reproducing the within-field variability can be expected.

In addition to the possible effect of the various stresses increasing the variability at the field scale, the assumption of a fixed value of HI could reduce the sensitivity of the model for reproducing this variability. The field data analyzed in this study pointed to a positive linear correlation between actual yield and HI ($r^2 > 0.8$) if the regression is analyzed for the average data obtained in each field as presented in Table 1. A similar phenomenon can be expected at the sub-field scale and probably the HI is correlated with final yield at the within-field scale. However, the correlation between HI and yield at each measurement location was not clear for every analyzed field. The r^2 for the linear correlation between HI and yield varied from 0.1 for field 2 to 0.99 for field 8. The narrow range of both magnitudes and the limited number of measurements in each field (3–9 measurements) could affect the significance of this correlation. In consequence, this study did not explore the

possible improvement of the proposed approach based on the variability of HI, but further studies should consider the implementation of operative approaches for the assessment of HI and its spatial distribution.

Additional sources of uncertainty, not directly attributable to the model, are the problems associated with the size and the shape of the fields. In general terms, the poorest performance was obtained in small fields (fields 6, 7) with an average size less than 6 ha. In these conditions, the signal captured in each pixel can be mixed with border areas and the accuracy of the yield monitor is affected working in short segments (Arslan and Colvin 2002b).

Evidence about the necessity of considering temporal evolution during the growing cycle for the assessment of the spatial variability

Additional evidence obtained in the analyzed fields demonstrated the necessity of considering the whole growing cycle for the assessment of the spatial variability and yield production rather than short periods or selected dates. For the irrigated fields analyzed in this work, the temporal evolution of the NDVI, or related variables, reached the maximum values during the stationary phase (plateau period). During this phase, the crop reached the maximum coverage and maximizes the rate of biomass accumulation (g of biomass per unit of time), but this period did not correspond with the maximum accumulated biomass in the field (g of biomass per unit of area). An example of this effect is provided in Fig. 6, comparing the temporal evolution of the NDVI for two areas (A and B) with different yield and similar maximum values of NDVI during the stationary phase. It is fair to say that most multispectral vegetation indices saturate for LAI values from 3 to 5 depending on the canopy architecture. Thus, the selection of more sophisticated indices such as LAI estimates based on neural networks or indicators based on hyperspectral sensors could provide higher sensitivity during the plateau. However, even considering the possible improvement of the indicators, the selection of single dates or short periods is seriously limiting for the assessment of variability at the subfield scale. According to the data, the differences obtained during determinate crop stages will not necessarily result in differences in crop production. The yield is the result of an accumulation process and the total values registered at harvest depend on the plant vigor and the length of the growing cycle. As presented in Fig. 6, the NDVI values and thus the accumulation of biomass can be displaced in time for the different areas. An example of this peculiarity is provided in Fig. 6, comparing the temporal evolution of NDVI for two areas (A and C). Area C had greater NDVI values (lower K_{cb} and crop expansion) during the phase of rapid growth (from March to May). In contrast, area A maintained greater values of NDVI during the crop senescence (late May and June). Consistently, both areas resulted in similar values of the accumulated transpiration coefficient and measured yield. Based on this evidence, it is expected that the estimates of yield diverge for other methodologies that consider only selected periods during the growing cycle.

Selection of thresholds for the definition of the growing cycle

The empirical evidence presented in this study demonstrated the necessity of considering the entire growing cycle for the assessment of spatial variability. Yield and biomass are dynamic processes, developed throughout the whole growing cycle and, as demonstrated in this work, the patterns of crop variability change during the cycle. An

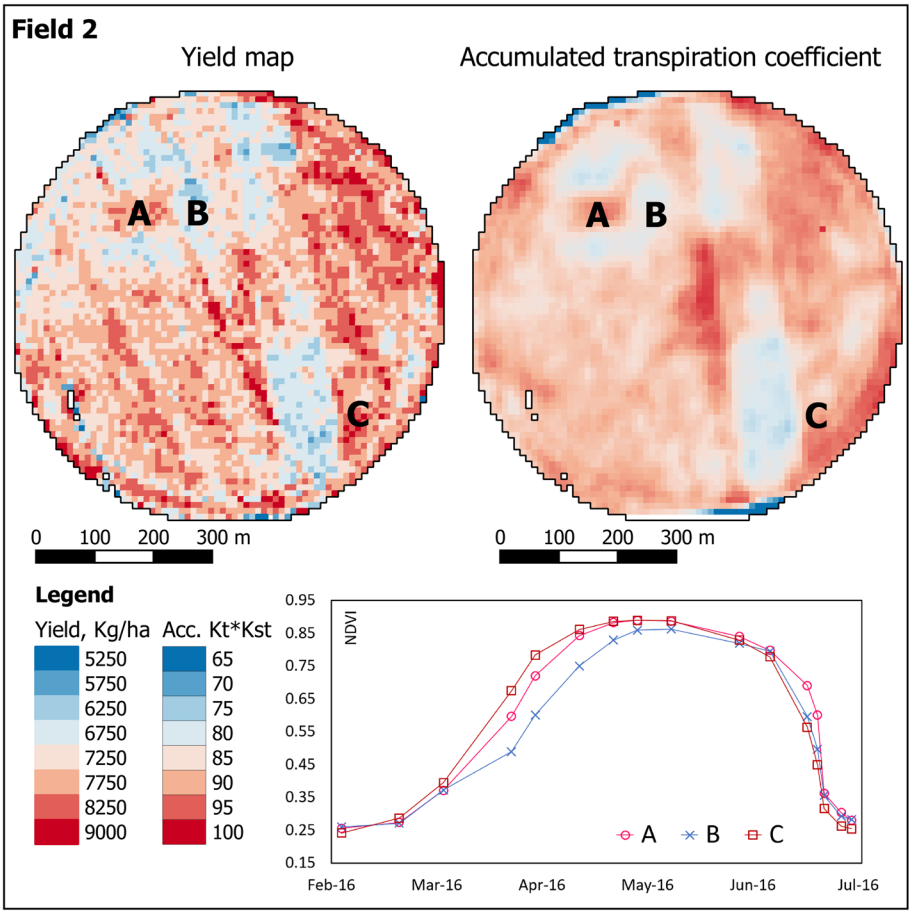

Fig. 6 Comparison of the spatial variability derived from grain monitors and the accumulated value of the transpiration coefficient (Kt). The lower graph represents the temporal evolution of NDVI in selected locations (A, B and C) for field 2

additional source of uncertainty is the selection of the beginning and end of the growing cycle. The results of the sensitivity analysis pointed to the relative advantage of the selection of t_0 and t based on NDVI thresholds. This method implicitly assumes that the particular conditions of each area (i.e. topography, soil albedo, orientation, soil composition) modify the microclimatic conditions affecting crop growth and development. Correspondingly, this methodology assumes that the effect of environmental stresses will be different in the diverse zones analyzed so crop growth and development will vary. These assumptions are not different to the conventions behind the use of VI thresholds for the definition of the crop cycle at the field scale proposed by Lobell et al. (2003) and basically the same principle was applied to different zones in the same field. The thresholds proposed in this work were based on the analysis of one field but are consistent with previous experiences determining the NDVI values at grain maturity in the study area (González-Gómez et al. 2018). However, it should be noted that more precise thresholds can be proposed for different management and development

conditions. In particular, the NDVI threshold considered for the end of the growing cycle could be excessive for rainfed fields with low canopy expansion.

Conclusions

The results obtained in this work corroborated the use of the accumulated value of K_t as a potentially sound method for the assessment of variability at sub-field scale. The values of accumulated K_t defined differences in crop growth similar to the biomass measurements and yield maps obtained for a wide range of management conditions and yield production. The assessment of within-field variability must be based on analysis of the whole growing cycle and the selection of the beginning and the end of the growing cycle based exclusively on RS data offered promising results.

The proposed approach improves on other methodologies for assessment of spatial variability. It can be applied in retrospective analysis using available databases of satellite images and maps can be obtained and analyzed during the season, providing a multi-annual series of crop heterogeneity. In addition, these results open the possibility for further interesting applications based on the characterization of field heterogeneity as is the case of variable rate irrigation and fertilization approaches.

Acknowledgements This research was developed in the framework of the projects HERMANA (HERramientas para el MAnejo sostenible de fertilización Nitrogenada y Agua), funded by the Spanish Ministry of Science and Innovation (AGL2015-68700-R) and FATIMA (FArming Tools for external nutrient Inputs and water MAnagement), funded by the European Union´s Horizon 2020 research and innovation programme (Grant Agreement No 633945). The authors of this paper are the persons that collaborate actively analyzing the data and preparing the manuscript, but we must acknowledge the effort of the persons involved in the data collection and processing (E. Sánchez from IDR-UCLM and F.M. Jara, I. Narro, F. Alonso, B. Quirós, H. Alcaraz, E. Pareja and P. Avilés from Instituto Técnico Agronómico Provincial) and the development of the software TONI (D. Guerrero from UCLM-IDR). The authors thank the three anonymous reviewers and the editor for their insightful comments and suggestions.

References

Allen, R.G., Raes, D., & Smith, M. (1998). *Crop evapotranspiration: Guidelines for computing crop requirements. Irrigation and Drainage Paper No. 56*. Rome, Italy: Food and Agriculture Organization.

Aparicio, N., Villegas, D., Casadesus, J., Araus, J. L., & Royo, C. (2000). Spectral vegetation indices as nondestructive tools for determining durum wheat yield. *Agronomy Journal, 92,* 83–91.

Arslan, S., & Colvin, T. S. (2002a). An evaluation of the response of yield monitors and combines to varying yields. *Precision Agriculture, 3,* 107–122.

Arslan, S., & Colvin, T. S. (2002b). Grain yield mapping: Yield sensing, yield reconstruction, and errors. *Precision Agriculture, 3,* 135–154.

Burke, M., & Lobell, D. B. (2017). Satellite-based assessment of yield variation and its determinants in smallholder African systems. *Proceedings of the National Academy of Science of the United States of America, 114,* 2189–2194.

Campos, I., González, L., Villodre, J., Calera, M., Campoy, J., Jiménez, N., et al. (2017a). Mapping within-field biomass variability: a remote sensing-based approach. In J. Taylor, D. Cammarano, A. Prashar, & A. Hamilton. *Proceedings of the 11th European Conference on Precision Agriculture, Advances in Animal Bioscience*. vol. 8, (pp. 764–769).

Campos, I., González-Gómez, L., Villodre, J., González-Piqueras, J., Suyker, A., & Calera, A. (2018). Remote sensing based crop biomass with water or light-driven crop growth models in wheat commercial fields. *Field Crop Research, 216,* 175–188.

Campos, I., Neale, C., Arkebauer, T., Suyker, A., & Gonçalves, I. (2017b). Water productivity and crop yield: A simplified remote sensing driven operational approach. *Agricultural Forest Meteorology, 249,* 501–511.

Campos, I., Neale, C., Suyker, A., Arkebauer, T., & Gonçalves, I. (2017c). Reflectance-based crop coefficients REDUX: for operational evapotranspiration estimates in the age of high producing hybrid varieties. *Agricultural Water Management, 187,* 140–153.

Chen, X., Vierling, L., & Deering, D. (2005). A simple and effective radiometric correction method to improve landscape change detection across sensors and across time. *Remote Sensing of Environment, 98,* 63–79.

Cicek, H., Sunohara, M., Wilkes, G., McNairn, H., Pick, F., Topp, E., et al. (2010). Using vegetation indices from satellite remote sensing to assess corn and soybean response to controlled tile drainage. *Agricultural Water Management, 98,* 261–270.

Dalla Marta, A., Grifoni, D., Mancini, M., Orlando, F., Guasconi, F., & Orlandini, S. (2013). Durum wheat in-field monitoring and early-yield prediction: assessment of potential use of high resolution satellite imagery in a hilly area of Tuscany, Central Italy. *Journal of Agricultural Science., 153,* 68–77.

Dang, Y. P., Pringle, M. J., Schmidt, M., Dalal, R. C., & Apan, A. (2011). Identifying the spatial variability of soil constraints using multi-year remote sensing. *Field Crop Research, 123,* 248–258.

Dixon, J., & McCann, M. (1997). *Precision Agriculture in the 21st century, Geospatial and information technologies in crop management*. Washington DC, USA: The National Academies Press.

Dobermann, A., & Ping, J. L. (2004). Geostatistical integration of yield monitor data and remote sensing improves yield maps. *Agronomy Journal, 96,* 285–297.

Duchemin, B., Hadria, R., Er-Raki, S., Boulet, G., Maisongrande, P., Chehbouni, A., et al. (2006). Monitoring wheat phenology and irrigation in central Morocco: On the use of relationships between evapotranspiration, crop coefficients, leaf area index and remotely-sensed vegetation indices. *Agricultural Water Management, 79,* 1–27.

Garcia, R., Kanemasu, E. T., Blad, B. L., Bauer, A., Hatfield, J. L., Major, D. J., et al. (1988). Interception and use efficiency of light in winter wheat under different nitrogen regimes. *Agricultural Forest Meteorology, 44,* 175–186.

González-Gómez, L., Campos, I., & Calera, A. (2018). Use of different temporal scales to monitor phenology and its relationship with temporal evolution of normalized difference vegetation index in wheat. *Journal of Applied Remote Sensing, 12*(2), 26010.

Ings, J., Mur, L. A., Robson, P. R., & Bosch, M. (2013). Physiological and growth responses to water deficit in the bioenergy crop Miscanthus x giganteus. *Frontiers in Plant Science, 4,* 468.

Iqbal, M. A., Shen, Y., Stricevic, R., Pei, H., Sun, H., Amiri, E., et al. (2014). Evaluation of the FAO AquaCrop model for winter wheat on the North China Plain under deficit irrigation from field experiment to regional yield simulation. *Agricultural Water Management, 135,* 61–72.

Jamieson, P. D., Porter, J. R., Goudriaan, J., Ritchie, J. T., Van Keulen, D., & Stol, W. (1998). A comparison of the models AFRCWHEAT2, CERES-Wheat, Sirius, SUCROS2 and SWHEAT with measurements from wheat grown under drought. *Field Crop Research, 55,* 23–44.

Jin, X. L., Feng, H. K., Zhu, X. K., Li, Z. H., Song, S. N., Song, X. Y., et al. (2014). Assessment of the AquaCrop model for use in simulation of irrigated winter wheat canopy cover, biomass, and grain yield in the North China plain. *PLoS ONE, 9*(1), e86938.

Jin, X., Li, Z., Yang, G., Yang, H., Feng, H., Xu, X., et al. (2017). Winter wheat yield estimation based on multi-source medium resolution optical and radar imaging data and the AquaCrop model using the particle swarm optimization algorithm. *ISPRS Journal of Photogrammetry and Remote Sensing, 126,* 24–37.

Lobell, D. B., Asner, G. P., Ortiz-Monasterio, J. I., & Benning, T. L. (2003). Remote sensing of regional crop production in the Yaqui Valley, Mexico: Estimates and uncertainties. *Agriculture, Ecosystems & Environment, 94,* 205–220.

Lobell, D. B., & Azzari, G. (2017). Satellite detection of rising maize yield heterogeneity in the U.S. Midwest. *Environmental Research Letters, 12,* 014014.

Lobell, D. B., Ortiz-Monasterio, J. I., Sibley, A. M., & Sohu, V. S. (2013). Satellite detection of earlier wheat sowing in India and implications for yield trends. *Agricultural Systems, 115,* 137–143.

Lobell, D. B., Thau, D., Seifert, C., Engle, E., & Little, B. (2015). A scalable satellite-based crop yield mapper. *Remote Sensing of Environment, 164,* 324–333.

Longnecker, N., Kirby, E. J. M., & Robson, A. (1993). Leaf emergence, tiller growth, and apical development of nitrogen-deficient spring wheat. *Crop Science, 33,* 154–160.

Maas, E. V., & Grieve, C. M. (1990). Spike and leaf development of sal-stressed wheat. *Crop Science, 30,* 309–1313.

Moran, M. S., Inoue, Y., & Barnes, E. M. (1997). Opportunities and limitations for image-based remote sensing in precision crop management. *Remote Sensing of Environment, 61,* 319–346.

Neale, C., Bausch, W., & Heerman, D. (1989). Development of reflectance-based crop coefficients for corn. *Transaction of the ASAE, 32,* 1891–1899.

Padilla, F. L. M., González-Dugo, M. P., Gavilán, P., & Domínguez, J. (2011). Integration of vegetation indices into a water balance model to estimate evapotranspiration of wheat and corn. *Hydrology and Earth Systems Science, 15,* 1213–1225.

Panda, S. S., Ames, D. P., & Panigrahi, S. (2010). Application of vegetation indices for agricultural crop yield prediction using neural network techniques. *Remote Sensing, 2,* 673–696.

Raes, D., Steduto, P., Hsiao, T., & Fereres, E. (2011). *Aquacrop reference manual*. Rome, Italy: Food and Agriculture Organization.

Ritchie, J. T., Singh, U., Godwin, D. C., & Bowen, W. T. (1998). Cereal growth, development and yield. In G. Y. Tsuji, G. Hoogenboom, & P. K. Thornton (Eds.), *Understanding options for agricultural production. Systems approaches for sustainable agricultural development* (pp. 79–98). Dordrecht, The Netherlands: Springer.

Sadras, V., Cassman, K., Grassini, P., Hall, A., Bastiaanssen, W., Laborte, A., et al. (2015). *Yield gap analysis of rainfed and irrigated crops: Methods and case studies. FAO water reports 41.* Rome, Italy: Food and Agriculture Organization.

Sibley, A. M., Grassini, P., Thomas, N. E., Cassman, K. G., & Lobell, D. B. (2014). Testing remote sensing approaches for assessing yield variability among maize fields. *Agronomy Journal, 106,* 24.

Stafford, J. V., Ambler, B., Lark, R. M., & Catt, J. (1996). Mapping and interpreting the yield variation in cereal crops. *Computers and Electronics in Agriculture, 14,* 101–119.

Steduto, P., Hsiao, T., Fereres, E., & Raes, D. (2012). *Crop yield response to water. FAO Irrigation and Drainage Paper No. 66.* Rome, Italy: Food and Agriculture Organization.

Steduto, P., Hsiao, T. C., & Fereres, E. (2007). On the conservative behavior of biomass water productivity. *Irrigation Science, 25,* 189–207.

Steduto, P., Raes, D., Hsiao, T. C., Fereres, E., Heng, L. K., Howell, T. A., et al. (2009). Concepts and applications of AQUACROP: the FAO crop water productivity model. In W. Cao, J. W. White, & E. Wang (Eds.), *Crop modeling and decision support* (pp. 175–191). Berlin, Germany: Springer.

Willmott, C. J. (1982). Some comments on the evaluation of model performance. *Bulletin of the American Meteorological Society, 63,* 1309–1313.

Willmott, C. J., Robeson, S. M., & Matsuura, K. (2012). A refined index of model performance. *International Journal of Climatology, 32,* 2088–2094.

Zwart, S. J., & Bastiaanssen, W. G. M. (2007). SEBAL for detecting spatial variation of water productivity and scope for improvement in eight irrigated wheat systems. *Agricultural Water Management, 89,* 287–296.